A Dual Resonant Microstrip Antenna for UHF RFID in the Cold Chain Using Corrugated Fiberboard as a Substrate

Mutharasu Sivakumar

B.E., Electronics and Communication Engineering,

St. Peter's Engineering College, Anna University,

India – May 2005

Master's Thesis

Submitted to the Department of Electrical Engineering and Computer Science and the Faculty of the Graduate School of the University of Kansas in partial fulfillment of the requirements for the degree of Master of Science in Electrical Engineering

Thesis Committee:

_____

Chairperson: Dr. Daniel Deavours

_____

Dr. Kenneth Demarest

_____

Dr. James Stiles

_____

Date defended: 01/24/2008

The thesis committee for Mutharasu Sivakumar certifies
That this is the approved version of the following thesis:

A Dual Resonant Microstrip Antenna for UHF RFID in the Cold Chain Using Corrugated Fiberboard as a Substrate

Thesis Committee:

_____
Chairperson: Dr. Daniel Deavours

_____
Dr. Kenneth Demarest

_____
Dr. James Stiles

_____
Date Approved: 01/29/2008

Abstract

Each year, about 76 million people contract a food borne illness in the United States; about 325,000 require hospitalization; and about 5,000 die. Tracking goods throughout the food supply chain increases the efficiency of recall of tainted goods and thus will help reducing food borne illness. Passive UHF RFID has been widely accepted to be a technology capable of increasing supply chain efficiency. Passive UHF RFID tags designed for supply chain application are tuned to work well on corrugated fiberboard boxes that are ubiquitous in the supply chain. Commercially available passive UHF RFID tags are either sensitive to the content/environmental conditions of the corrugated fiberboard box or economically unfeasible. In this thesis we propose a novel dual-resonant planar UHF RFID microstrip antenna designed to be both insensitive to the content/environmental conditions of the corrugated fiberboard box and economically feasible. We provide simulated performances and experimental validations to show that the proposed microstrip antenna design is a viable and technically superior solution compared to conventional stripline dipole antennas widely used in commodity tags.

Acknowledgement

I thank my advisor Dr. Daniel Deavours for his guidance and encouragement that has helped me to successfully complete my thesis and my graduate study at The University of Kansas. I also thank him for giving me the opportunity to work with him at the RFID Alliance Lab. He has been a wonderful teacher and a tremendous inspiration.

I thank Dr. Kenneth Demarest and Dr. James Stiles for being in my thesis committee. I sincerely believe that their suggestions and feedback will add a lot of value to my thesis. I also thank them for every thing they have thought me in the class room.

I thank Information and Telecommunication Technology center and Department of Electrical Engineering and Computer Science at The University of Kansas for giving me this wonderful opportunity to learn and master my skills as an Electrical Engineer.

I thank all the graduate students who worked with me in the RFID Alliance Lab for their help and support.

To my family and friends

Table of Contents

List of Figures

List of Tables

1. Introduction

According to a report released by the U.S. Government Accountability Office in April 2007 [1], each year, about 76 million people contract a food borne illness in the United States; about 325,000 require hospitalization; and about 5,000 die. Food contamination (e.g., E. coli in spinach, Salmonella in peanut butter) is one of the major reasons for food borne illness [1]. Reducing the consumption of such tainted food has become an absolute necessity for reducing food borne illness. One of the important steps involved in reducing the consumption of tainted food is to identify and recall all the goods that are suspected to be tainted. Tracking goods throughout the food supply chain increases visibility and hence improves the efficiency of recalling the tainted goods. Passive UHF RFID has been widely accepted to be a technology capable of increasing supply chain efficiency [2]. But the food supply chain (more commonly called cold chain) poses unique challenges that limit the use of passive UHF RFID.

Passive UHF RFID tags designed for supply chain application generally use stripline dipole antennas and are tuned to work well on corrugated fiberboard boxes due to their ubiquitousness in the supply chain. The consumer packaged goods (CPG) industry typically ships goods in relatively stable environmental conditions. Furthermore, the majority of CPG goods are “RF friendly” in that they do not contain metal or water, or they have suitable air gaps that make tagging possible. In contrast, the cold chain

applications frequently have liquid contents, and the environmental conditions can vary widely from being freeze-dried to being filled with wet produce in the field. It is well known that the performance of passive UHF RFID tags degrade when the corrugated fiberboard container has water content [3] [4]. These challenges are one of several reasons why RFID tagging in cold chain has lagged the CPG market, even though the potential advantages of RFID on reduced shrinkage and improved food safety are clear.

One commonly used solution for tagging objects in proximity to materials with extreme dielectric properties (like water) is the use of a microstrip antenna [6] [7] [8] instead of the conventional stripline dipole antenna. The inherent ground plane present in a microstrip antenna acts as a shield from any material present behind the antenna and hence provides a feasible solution for tagging any object. One of the limitations of using a microstrip antenna instead of a stripline antenna is the larger profile of a microstrip antenna. Microstrip antennas are usually multiple layered structures that are thick and they commonly require metallic connections between the layers [6] [7] and hence are complex and expensive to manufacture.

The limitation of large profile of microstrip antennas can be overcome by using corrugated fiberboard as the substrate. This way the tag antenna can be manufactured using a conventional stripline antenna manufacturing process and a metal foil can be provided inside the corrugated fiberboard container, thus constructing the microstrip antenna. Such a construction requires the antenna to have a completely planar structure [8] i.e., does not require a connection between the antenna plane and the ground plane.

This approach would be better than using a stripline dipole antenna due to the shielding provided by the ground plane, but is still impractical because corrugated fiberboard is very hygroscopic (readily absorbs water).

Large variations in water content of the corrugated fiberboard due to change in temperature and humidity conditions results in a large change in dielectric properties of the substrate. Traditional microstrip approach [8] fails to maintain a consistent performance over various temperature and humidity conditions due to its limited bandwidth.

Furthermore, increased use of RFID in supply chain requires multiple readers to operate in close proximity. In such an environment it is necessary to control the reader's field of operation such that the reader only reads the tags that are intended to be read. We call this the near-far problem. For example, reader in one conveyor belt must not read tags in the adjacent conveyor belts. The reader output power is reduced considerably in order to achieve a controlled read zone. Latest improvements in UHF RFID tags continually increase tags' ideal condition performance, but, the tag's non-ideal condition performance is still highly degraded. This, along with reduced reader output power results in highly unreliable system. Therefore, an ideal solution would be a tag that delivers a consistent, high level of performance regardless of the contents of the corrugated fiberboard container and variations in the temperature and humidity conditions. Such a tag does not currently exist.

In this thesis, we propose a novel microstrip antenna that uses the corrugated fiberboard as the substrate and is designed to adapt to a wide range of dielectric properties that corrugated fiberboard may reasonably take. To do this, we propose the use of two physically separate antennas and a novel but simple matching circuit. The antennas and matching circuit are designed to provide an even, modest level of performance over a very wide range of dielectric properties.

2. Background

2.1. Corrugated Fiberboard

Corrugated fiberboard, commonly called "cardboard," can be classified based on the number of paper walls, the thickness, and density of the flutes. Fiberboard commonly comes in three forms: single faced, in which flutes have paper all on one side; single walled, in which flutes are sandwiched between paper walls; and double walled, in which two layers of flutes are contained by three paper walls. Single-walled fiberboard is the type most commonly used in the cold chain.

Fiberboard can also be classified in the type of flutes and number of flutes per unit length. The "C" flute is the most common form of corrugated fiberboard with flute density of 42 flutes every 12 inches. For this paper, we use a sample of "C" flute corrugated fiberboard that is 0.150 inches (3.81 mm) thick.

2.2. Tag performance reduction in proximity to water

The performance reduction of passive UHF RFID tags that use stripline dipole antennas in proximity to water has been studied in [9]. Figure 1 shows the performance reduction due to the presence of water inside a corrugated fiberboard container for the four different tags with different form factors. These results indicate the limitation of using commodity tags that use

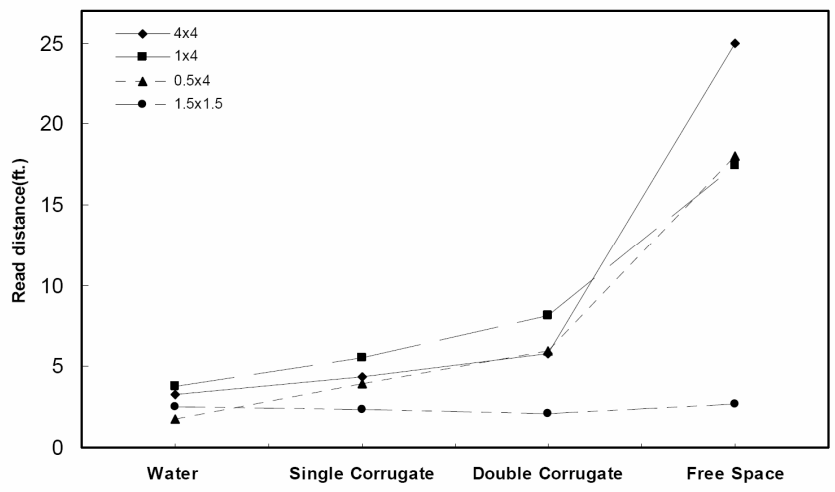

Fig. 1: Read distance of tags near water [9]

stripline dipole antennas for supply chain application. It is important to note that these results were taken in room temperature conditions. Change in temperature and humidity conditions results in variations in the water content of the corrugated fiberboard and may result in even more drastic performance reduction.

2.3. Moisture in Corrugated Fiberboard

Using a microstrip antenna for a UHF RFID tag is a possible solution to tag high dielectric substances like water. But, due to size and cost constraints using corrugated fiberboard as the antenna substrate proves to be a viable option. The primary limitation of corrugated fiberboard as a substrate for a microstrip antenna is that fiberboard is hydroscopic. Thus, the dielectric properties of corrugated fiberboard change based on temperature, humidity,

and history. Higher water contents cause corrugated fiberboard to have a larger dielectric constant, affecting the resonant frequency, and a larger dissipation factor, affecting the antenna efficiency and impedance. Water content of fiberboard follow a sorption / desorption isotherm [3]. When the relative humidity increases, the sorption rate is used to calculate the moisture content, and when the relative humidity decreases, desorption rate is used. Table 1 illustrates a typical sorption / desorption isotherm. The water content can vary between 6 g and 18 g/100g between 40%-90% relative humidity. According to [5], equilibrium moisture content of single walled corrugated fiberboard at 20 degree Celsius and 54.4% relative humidity is 9.34g/100g of solid substance [5]. Under similar conditions, we measured our sample of corrugated fiberboard to have water content of about 6.5g/100g. From this, we can assume that a microstrip antenna needs to tolerate water contents ranging between 6g/100g and 18g/100g. Cold chain environments can be even more demanding. If the temperature drops below freezing, the water content can be freeze-dried out of the corrugated fiberboard, making the moisture content effectively 0g/100g. Melted frost or other environmental forms of moisture may cause even higher moisture levels. We target the range of moisture contents to be between 0g/100g and 25g/100g.

Table 1: Sorption / desorption of fiberboard [3]

Temp.	40% RH	90% RH
1° C	8 g/100g (Sorption) 10 g/100g (Desorption)	16 g/100g (Sorption) 18 g/100g (Desorption)
40° C	6 g/100g (Sorption) 10 g/100g (Desorption)	14 g/100g (Sorption) 18 g/100g (Desorption)

2.4. Dielectric Properties of Corrugated Fiberboard

Water has a large dielectric constant (approximately 80) and loss tangent (approximately 0.5) at 900 MHz. Consequently, changes in water content of corrugated fiberboard will have a significant impact on the dielectric properties of corrugated fiberboard. Note that water is absorbed by the fiberboard and loosely bound to the fiberboard, and does not behave as liquid water. Therefore, we can not use a simple proportionality calculation to measure the dielectric properties of corrugated fiberboard, so the dielectric properties must be measured. In order to measure the dielectric properties of corrugated fiberboard for various water contents we used the microstrip antenna method [10]. We first constructed a microstrip antenna for a known dielectric substrate and simulated the impedance of the antenna in a finite element simulation tool (Ansoft HFSS). We then replaced the substrate by the unknown substrate and recorded the impedance using a network analyzer. Then by changing the dielectric properties of the substrate in the simulator, the simulated impedance was matched to the measured impedance. The dielectric properties of the substrate that achieves this match are the actual dielectric properties of the unknown dielectric substrate. Using this method dielectric property of corrugated fiberboard was found for different water contents. The measured dielectric properties of corrugated fiberboard are tabulated in Table 2.

Table 2: Measured dielectric properties of corrugated fiberboard

Water content (g/100g)	ε_r	tan δ
~0	1.22	0.005
6.5	1.28	0.007
10	1.35	0.016
18	1.4	0.027
25	1.5	0.038

2.5. Power Waves and the Scattering Matrix

UHF RFID tags communicate with the reader using backscatter principle. The chip in the tag harvests the RF power transmitted by the reader in order to provide power supply for the chip. The chip uses this power to switch between two impedance states. This change in impedance state modulates the signal backscattered by the RFID tag antenna and tag uses this to communicate back to the reader. The chip uses diodes in order to harvest the RF power and hence has complex input impedance. The UHF RFID tag antenna that is directly connected to the chip should therefore have conjugate matching impedance to that of the chip in order to have the maximum power transfer efficiency.

Since we have complex source and load impedances S_{11} is not the appropriate metric for power transfer. Power transfer is governed by power transfer efficiency 'τ' given by the following expression [11].

$$\tau = \frac{4R_c R_a}{\left|Z_c + Z_a\right|^2}, \quad 0 \le \tau \le 1. \tag{1}$$

When $R_c = R_a$ and $X_c = -X_a$, then $\tau = 1$ and this is the condition of conjugate match and 100% power transfer efficiency. Since S_{11} is not the metric for power transfer, using a smith chart normalized to 50 Ohm does not provide an intuitive understanding of the power transfer efficiency [12]. Kurokawa [12] devised a method for using the smith chart to plot the power transfer efficiency using the power wave reflection coefficient for complex load s that is the fraction of power that is not delivered to the load from the generator. The power wave reflection coefficient for a complex load is given by the following expression.

$$s = \frac{Z_a - Z_c^*}{Z_a + Z_c^*}, \quad 0 \leq |s|^2 \leq 1. \tag{2}$$

It can be shown that $\tau + |s|^2 = 1$. Now we can define a conformal transform,

$$\hat{z}_a = \frac{R_a}{R_c} + j\frac{X_a + X_c}{R_c} \tag{3}$$

Such that $\hat{z}_a$ defines a valid smith chart transformation

$$\hat{z}_a = \frac{1+s}{1-s} \tag{4}$$

We call this Smith chart transformation a *power wave Smith chart*, in which, a fixed value of power transfer efficiency traces a circle around the center of the smith chart whose radius is equal to the magnitude of the power reflection coefficient vector *s*. This provides a pictorial representation of the quality of the impedance matching for the antenna. The center of the smith chart now represents a power transfer efficiency $\tau = 1$. The unit circle of the smith chart now represents a power transfer efficiency $\tau = 0$.

2.6. Q factor of a dipole near a ground plane

A commodity tag usually made using an electrically short stripline dipole can be tuned to work efficiently in proximity to metal but suffers from reduced bandwidth. It is common to rate the quality of a reactive element, such as a capacitor or inductor, by the quality factor, or Q. Generally, $Q = \omega \frac{EnergyStored}{PowerDissipated}$. For antennas, Q is an important metric because it is inversely proportional to bandwidth. Formally, $BW = \frac{f_0}{Q}$, where f_0 is the resonant frequency of the antenna and BW is the range of frequencies over which the energy stored in the system is at least half of the energy stored at the resonant frequency. Energy is stored within an antenna through the capacitance and inductance of the elements of the antenna. Energy can be dissipated either through radiation, sometimes called radiation resistance, or through other losses, such as Ohmic losses on conductors and dielectric loss.

A narrow-wire half-wave dipole has a $Q \approx 6$ [13]. i.e., a half-wave dipole with resonant frequency at 915 MHz would have approximately 150 MHz of bandwidth, which is more than adequate for world-wide operation. A resonant-length dipole at 915 MHz is approximately 6.1 inches long, which is too long for many applications. It is common for dipoles to be short enough to fit on a 4 inch label, i.e., 3.75 inches. The radiating Q of such a short dipole is approximately 40 [13], or about 23 MHz of bandwidth. The radiating Q of such a short dipole near a metal ground plane is approximately 80 [14], or about 12 MHz of bandwidth, which is adequate for operation over the FCC-allowed spectrum. But a change of dielectric constant form 1.22 to 1.5 shifts the resonant frequency more than 80 MHz. This clearly proves that a narrow-wire half-wave dipole antenna (most commonly used in commodity tags) does

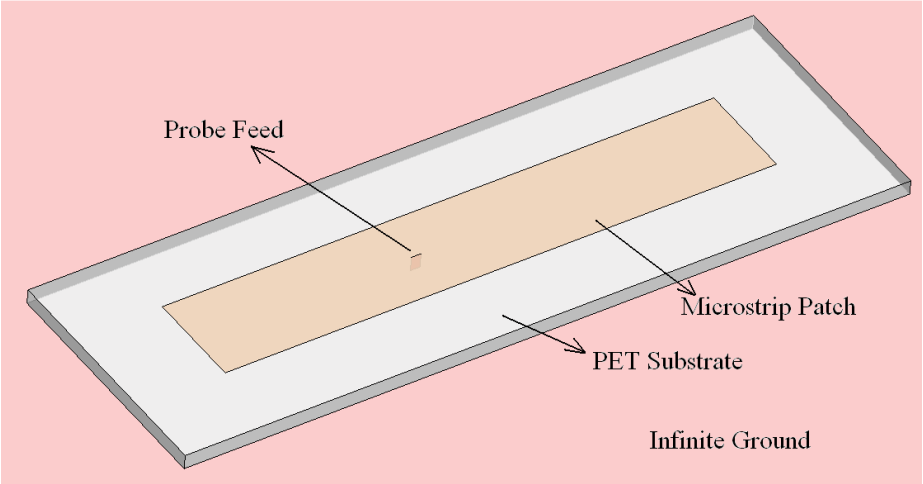

Fig. 2: Probe fed rectangular microstrip antenna

not have the required bandwidth to operate over the dielectric property range specified in Table 2 and hence, cannot be a viable solution for tagging corrugated fiberboard containers in cold chain.

2.7. Surface Currents on a Rectangular Microstrip Antenna

A probe fed rectangular microstrip antenna (see Figure 2) was simulated using a finite element tool to investigate the impedance and surface currents. A copper microstrip patch with dimensions 114 mm×20 mm was simulated on a 150 mm×50 mm×1.62 mm polyethylene substrate over an infinite copper ground plane. The antenna was fed with a probe feed, 10 mm from the center, exciting the TM_{10} mode. The antenna had a self-resonant frequency of about 893 MHz. The input impedance Z_A obtained from the simulation is shown in Figure 3. Figure 4 shows the phase of the input impedance Z_A. Defining bandwidth as frequencies at which $\angle Z_A$ is less than

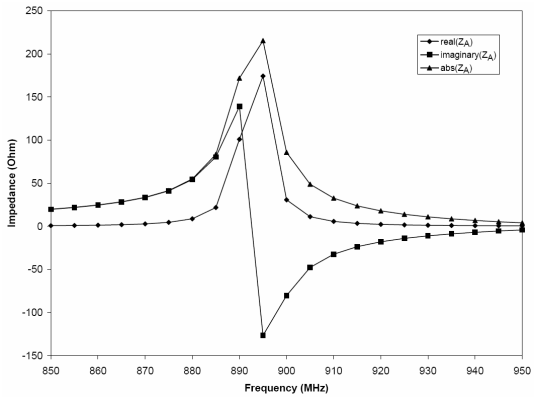

Fig. 3: Input impedance of the microstrip antenna in Fig. 3

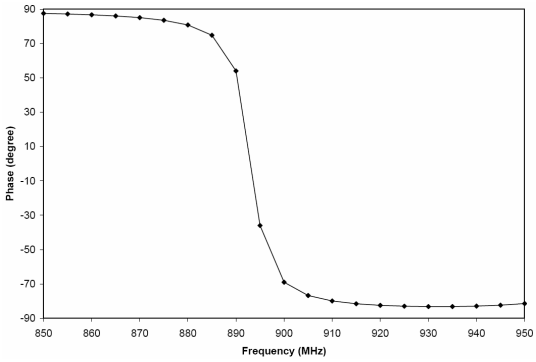

Fig. 4: Phase of input impedance shown in Fig. 4

45˚, we see that the microstrip antenna in Fig. 2 has a bandwidth of about 5 MHz. Inspecting the phase of the antenna in Fig. 5 we can see that phase of the input impedance is always less than -45˚ above 898 MHz (i.e., 1 bandwidth) and the phase is always greater than 45˚ below 888 MHz (i.e., 1 bandwidth). The phase of surface current on the microstrip patch follows this change in phase of the impedance. This characteristic of a microstrip patch antenna plays an important role in the design of the proposed dual-resonant antenna. This has been discussed in further detail in Chapter 3.

3. Design

3.1. Design Constraints

Read distance of an RFID tag is mainly limited by the total "realized gain" of the RFID tag antenna. We have a load with complex impedance attached to the antenna. Therefore, the *realized gain* in this context is defined by the following expression.

$$G_R = D\eta\tau \tag{5}$$

Here, η is the radiation efficiency of the antenna; τ is the power transfer efficiency defined by (1) and D is the directivity of the antenna. The terms η and τ take values between 0 and 1. D may vary with design constraints like size and the type of antenna used. However, for maximum performance, we must maximize the product $\eta\times\tau$ over the operating frequency range in order to get the best G_R.

In Chapter 1 we defined an ideal tag antenna for cold chain application as: a tag that has a constant maximum read distance i.e., realized gain, irrespective of the changes in water content of the corrugated fiberboard. This is a qualitative definition. Designing an antenna for this constraint requires a more quantitative definition.

Now, the Directivity of the antenna *D(w,f)* is a function of frequency *f* and water content *w*. For simplicity, we choose to solve the problem at a single frequency f = 915 MHz. The directivity of the tag *D(w,915 MHz)* does

not change substantially with change in water content *w*. Therefore, to maintain a constant realized gain over the various water contents we are required to maintain the *Effective Efficiency* $\eta_{eff}(w,915\ MHz)=\eta\ (w,915\ MHz)\times\tau(w,915\ MHz)$ a constant with respect to the change in water content *w* of the corrugated fiberboard. From now on, our whole analysis is at f = 915 MHz, unless specified. The dielectric loss in the antenna is one of the main factors affecting the efficiency of the antenna $\eta(w)$. Since the dielectric loss is the highest at 25g/100g water content (see Table 2), $\eta(w)$ is the least at w = 25g/100g. This is an upper bound at w = 25g/100g. Based on this, we formally define our design constraint as

$$\alpha\eta_{eff}(25g/100g) \geq \eta_{eff}(w) \geq \beta\eta_{eff}(25g/100g), \quad 0g/100g \leq w \leq 25g/100g \tag{6}$$

Where, α and β are bounds on performance that are ideally required to be unity. We also chose a form factor of 45 mm x 145 mm as a self imposed size constraint for the tag. This is a form factor similar to that of a commodity tag chosen for comparison later on.

3.2. Radiation Efficiency of the Antenna

Radiation efficiency of an antenna is the ratio of power radiated by the antenna to the total power input to the antenna. Radiation efficiency of a microstrip patch antenna can be calculated from *Q* of the antenna as shown in (7) [14].

$$\frac{1}{\eta} = Q_r\left(\frac{1}{Q_r}+\frac{1}{Q_d}+\frac{1}{Q_c}+\frac{1}{Q_{sw}}\right) \tag{7}$$

$$Q_r = \frac{2\pi f W_{es}}{P_r} \tag{8}$$

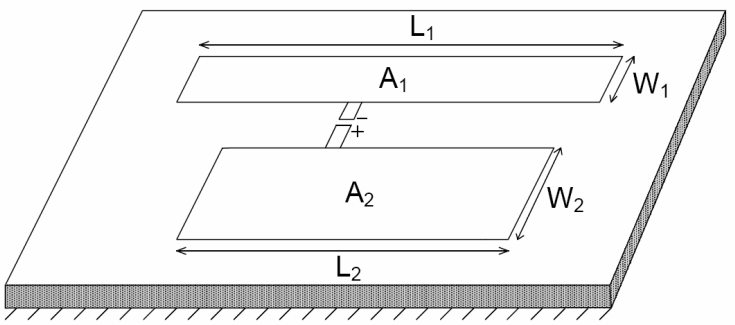

Fig. 5: Dual Patch Antenna Dimensions

From (7) we can say that in order to maximize the radiation efficiency η we are required to minimize Q_r and maximize Q_d, Q_c and Q_{sw}. For a rectangular patch antenna Q_d, Q_c and Q_{sw} are not affected by width of the patch [14]. According to (8) [14] Q_r is directly proportional to energy stored W_{es} and inversely proportional to power radiated into space P_r. W_{es} is directly proportional to the width of the patch antenna and P_r is directly proportional to the square of the width of the patch antenna [14]. Therefore, a wider patch antenna has a lower Q_r than a narrower patch antenna. Hence we can conclude radiation efficiency η of a wider patch antenna is larger than that of a narrower patch antenna with all else the same.

The microstrip antenna design proposed (see Figure 5) has two patches that have different lengths and resonant frequencies at least 3 bandwidths away from each other. The longer patch, A_1 is tuned in frequency to be efficient for the lower water contents i.e., lower relative permittivity. Since the dielectric loss is less for lower water contents, a narrower patch is sufficient to keep the radiation efficiency high. The shorter patch, A_2 is tuned in frequency to be efficient for higher water contents, i.e., higher relative permittivity. Since the dielectric loss is high for higher water contents, a wider patch is used in order to keep the radiation efficiency high.

Table 3: Phase of the input impedance at different frequency regions

Region 1	$f < f_1$	$\angle Z_{A1}^{\circ} > 45°$	$\angle Z_{A2} > 45^{\circ}$
Region 2	$f = f_1$	$\angle Z_{A1} = 0^{\circ}$	$\angle Z_{A2} > 45^{\circ}$
Region 3	$f_1 < f < f_2$	$\angle Z_{A1} < -45^{\circ}$	$\angle Z_{A2} > 45^{\circ}$
Region 4	$f = f_2$	$\angle Z_{A1} < -45^{\circ}$	$\angle Z_{A2} = 0^{\circ}$
Region 5	$f > f_2$	$\angle Z_{A1} \approx< -45^{\circ}$	$\angle Z_{A2} < -45^{\circ}$

Since we have two separate radiating elements in the antenna that are resonant at frequencies a few orders of bandwidth away from each other, there exists frequency at which the surface currents in the two antennas are out of phase. The surface currents drive the fringing E-fields that in turn generate the radiated TEM waves. When the surface currents in the two patches are out of phase, the resulting TEM waves degenerate in the far-field resulting in reduced efficiency and an irregular radiation pattern. Therefore, it is necessary to investigate the frequency at which this occurs and avoid this from happening at the required operating range of the antenna.

Let the input impedance of antennas A_1 and A_2 be Z_{A1} and Z_{A2} respectively. When the self-resonant frequencies of the two patches are sufficiently far away in frequency (few orders of bandwidth) we can define five distinct frequency regions as shown in Table 3.

In Region 3 as defined in Table 3, A_1 is above its resonance and A_2 is below its resonance and this creates approximately 180° phase difference between the surface currents of the two patches (see section 2.7). There is an additional 180° phase difference between the surface currents as the patches are fed differentially. Therefore, the net phase difference of the surface

currents of the two patches is ≈0°. This is applicable only if both the antennas are fed to the same side from their center. Since there is no phase difference between the surface currents in the two patches, the fringing fields of the two patches are in phase as shown in Figure 6. Since the fringing fields are in phase, the TEM waves generated by the fringing fields add constructively in the far-field. A similar investigation of Region 1 and Region 5 as defined in Table 3 shows that the currents in the two patches are 180° out of phase. Although this causes the TEM waves to degenerate in the far-field, at least one of the antennas is very far from its resonance and has very negligible surface currents resulting in weak fringing fields that do not affect the radiation of the other antenna that is close to its resonance. Thus we can conclude that it is reasonable to operate the antenna in all the five frequency regions provided both the antennas are fed to the same side from their centers.

If instead we choose to feed one antenna to the left of its center and the other antenna to the right of its center, the degeneration of the TEM waves happens in Region 3 and the antenna will not be capable of operating efficiently in this frequency region.

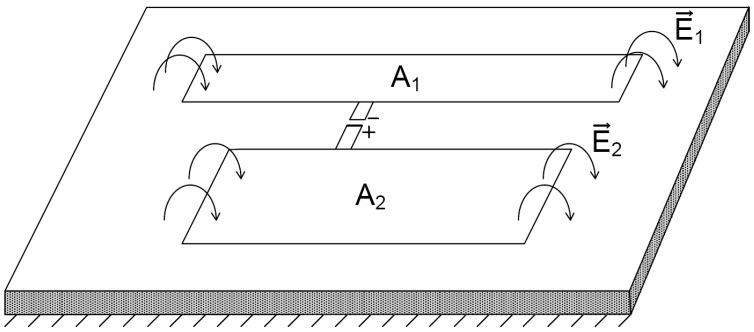

Fig. 6: E-fields on the two radiating patches in Region 3 when both the patches are fed left of center

3.3. Power Transfer Efficiency of the Antenna

Although the poor radiation efficiency of the antenna at high water contents is compensated by compromising the width of the two patches, the radiation efficiency is still least at the highest water content w = 25g/100g. Now, according to the design constraint specified in (6) we are required to maintain the product of radiation efficiency η and the power transfer efficiency τ a constant. This can be achieved by suitably designing the matching circuit of the antenna. The matching network must connect both the patches to the chip in a completely planar structure and also provide the required impedance match that achieves a constant realized gain.

The matching network is constructed using 2 mm wide microstrip transmission lines that have a characteristic impedance of approximately 150 Ω at 6.5g/100g water content. The microstrip transmission lines are used to transform the impedance at the feeding edge of the radiating patches to provide conjugate matching impedance to the RFID chip. The impedance at the feeding edge of the antenna can be obtained using the transmission line model [15] of a rectangular patch antenna show in Figure 7.

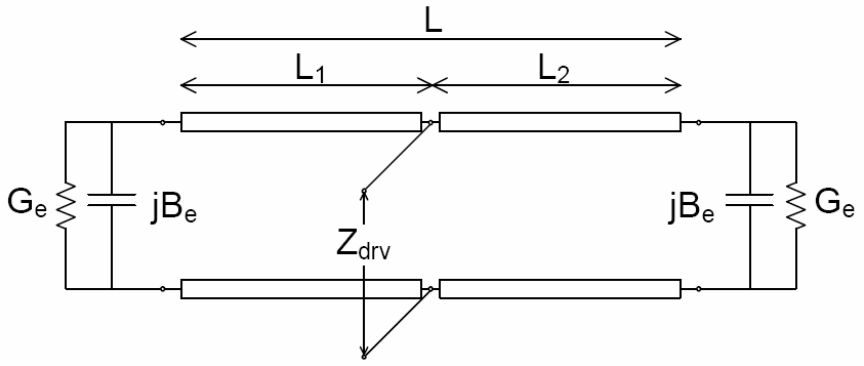

Fig. 7 Transmission Line Model of a Rectangular Patch Antenna [15]

According to the transmission line model [15] of a rectangular microstrip antenna the driving point impedance is a function of the lengths L_1 and L_2. At resonance, $L = \lambda/2$ and the radiation resistance is large. Therefore, when $L_1 = L_2$ the driving point impedance $Z_{drv} \approx 0\Omega$ and as the difference between L_1 and L_2 increase the driving point impedance increases according to the following equation.

$$\frac{1}{Z_{drv}} = Y_{drv} = Y_o \left[\frac{Y_e + jY_o \tan(\beta L_1)}{Y_o + jY_e \tan(\beta L_1)} + \frac{Y_e + jY_o \tan(\beta L_2)}{Y_o + jY_e \tan(\beta L_2)} \right]$$

$$Y_e = G_e + jB_e$$

Where; G_e is the conductance associated with the power radiated, B_e is the susceptance due to the energy stored in the fringing field near the radiating edge, Y_o is the characteristic admittance of the transmission line (the rectangular patch antenna in this case) and β is the propagation constant of the transmission line.

The driving point impedance Z_{drv} is transformed by a short microstrip transmission lines that is primarily designed to add reactance to the impedance. This impedance transformation is governed by the transmission line equation [16]. The two microstrip patch antennas are attached to the chip

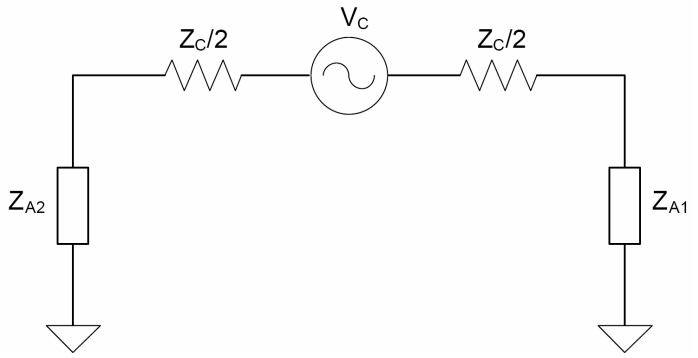

Fig. 8: Equivalent circuit of dual-resonant antenna

using microstrip transmission lines. The equivalent circuit of the antenna is shown in Figure 8. The impedance Z_{A1} and Z_{A2} represent the impedances at the feeding edges of Antenna 1 and Antenna 2 respectively transformed by the microstrip transmission lines. Z_C is the complex impedance if the UHF RFID chip.

At lower water contents Antenna 1 operates close to its resonance and Z_{A1} is the rectangular patch antenna impedance transformed by the transmission line. At these water contents Antenna 2 is far away from it resonance and the impedance transformed by the transmission line is primarily reactive. These two impedances are in series and the resulting impedance Z_A must be a complex conjugate of the chip impedance Z_C in order to have perfect power transfer between the antenna and the chip.

The antenna impedance Z_A can be changed by suitably changing the location of the feeding edge in the antennas and the lengths of transmission lines attaching the chip to the feeding edge of the patch antennas. At lower water contents we intentionally keep the loss of power due to impedance mismatch relatively high because efficiency of the antenna is relatively high in the low water content scenario. Keeping the power loss due to impedance mismatch high is necessary for maintaining the same realized gain for all the water contents. Now as the water content increases efficiency of the antenna decreases and this is compensated by increasing τ i.e. decreasing the power lost due to impedance mismatch.

3.4. Simulated Results

The antenna (shown in Figure 9) was designed and simulated using an electromagnetic simulation tool based on finite element method (FEM) [17] for five different dielectric properties given in Table 2. The simulated

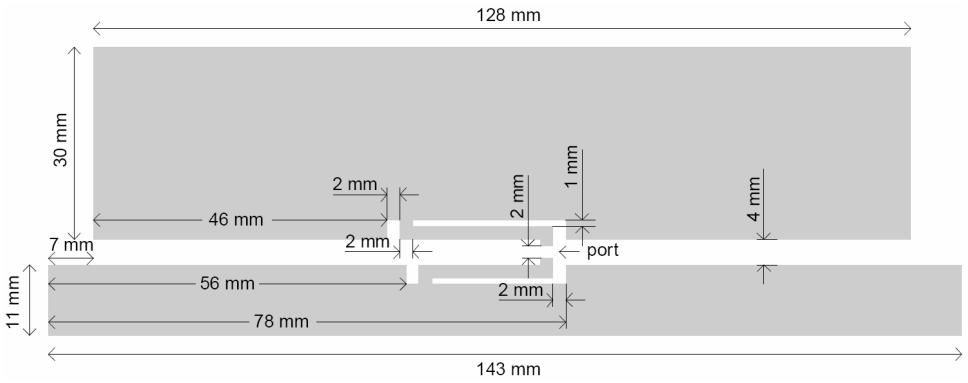

Fig. 9: Outline of the proposed dual resonant microstrip antenna (substrate and ground plane not shown here)

impedance at various water contents is plotted in a power wave smith chart shown in Figure 10. The plot shows the impedance between 890 MHz and 940 MHz at 2 MHz interval. The solid square indicates the impedance at 890 MHz for every value of water content.

The simulated directivity, radiation efficiency, power transfer efficiency and realized gain of the proposed antenna design are given in Figure 11 for all the water contents. Note that the directivity of the antenna remains fairly constant with respect to change in water content and the radiation efficiency η decreases as the water content increases. The power transfer efficiency τ has been suitably adjusted to obtain a fairly constant realized gain G_R. The antenna parameters achieve the performance bound of (6) with an α=1.31 and a β=0.812. In other words the simulated $\eta_{eff}(w)$ of the proposed antenna has ~±1 dB deviation from $\eta_{eff}(25g/100g)$. Therefore, we have achieved a simulated tag antenna performance that effectively eliminates the near-far problem as mentioned in Chapter 1.

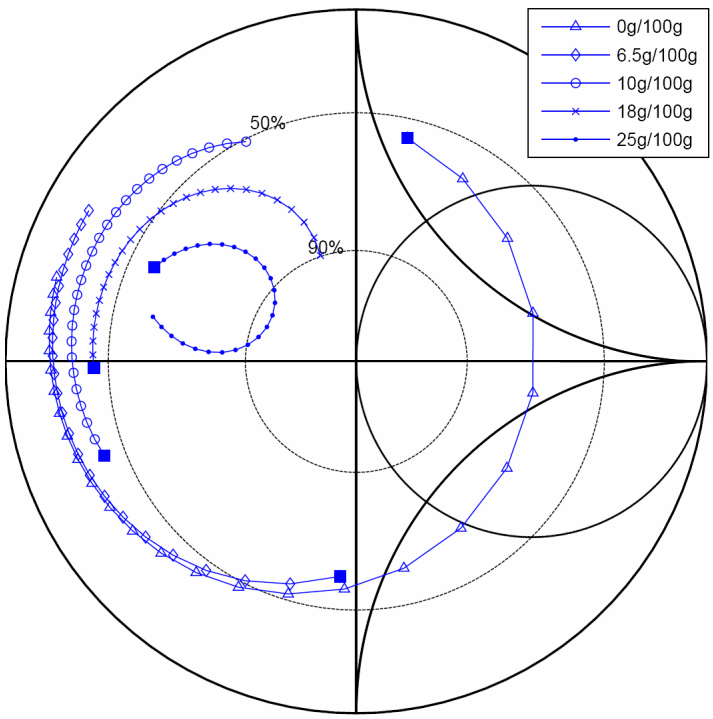

Fig. 10: Simulated impedance plotted in a power wave Smith chart normalized to 35-j110 Ω

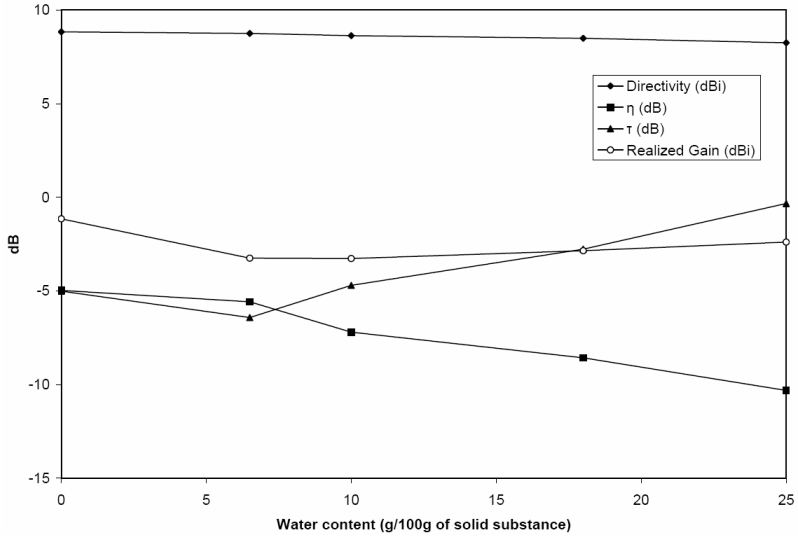

Fig. 11: Simulated antenna parameters at 915 MHz

The surface currents in the two patches at a frequency of 915 MHz were obtained from simulation at three different water contents. The antenna operates in Region 3 as shown in Table 3 at all the water contents.

At very low water contents the longer patch is close to its resonance. Therefore, at lower water contents only the surface current in the longer patch is significant and hence contribute towards radiation in the far field. The shorter patch has lower surface current and hence has negligible contribution towards radiation in the far field. The surface current for 0g/100g water content is plotted in Figure 12.

At very high water contents the shorter patch is close to its resonance. Therefore, at high water contents surface current in the shorter patch is high compared to the longer patch. Therefore, the shorter patch has relatively high contribution to the far field radiation compared to the shorter patch. The surface current for 18g/100g water content is plotted in Figure 13.

At water contents between the extremes, both the patches are active

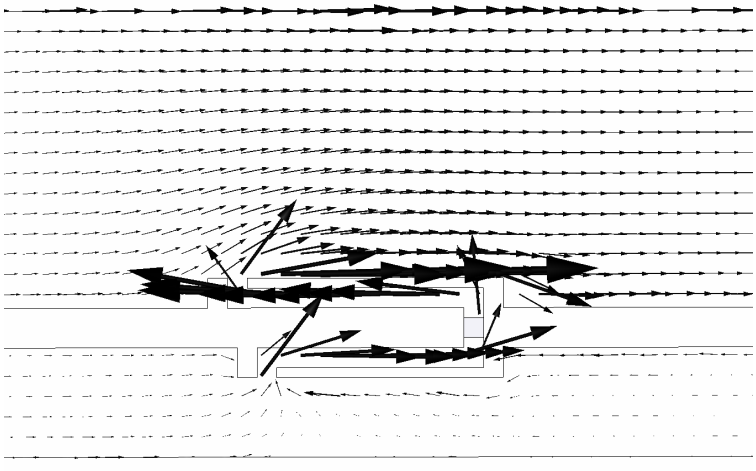

Fig. 12: Surface currents at 18g/100g

and hence surface current in both the patches contribute towards radiation in the far field. The surface current for 10g/100g water content is plotted in Figure 14. It can be observed that the currents in both the patches have the same phase.

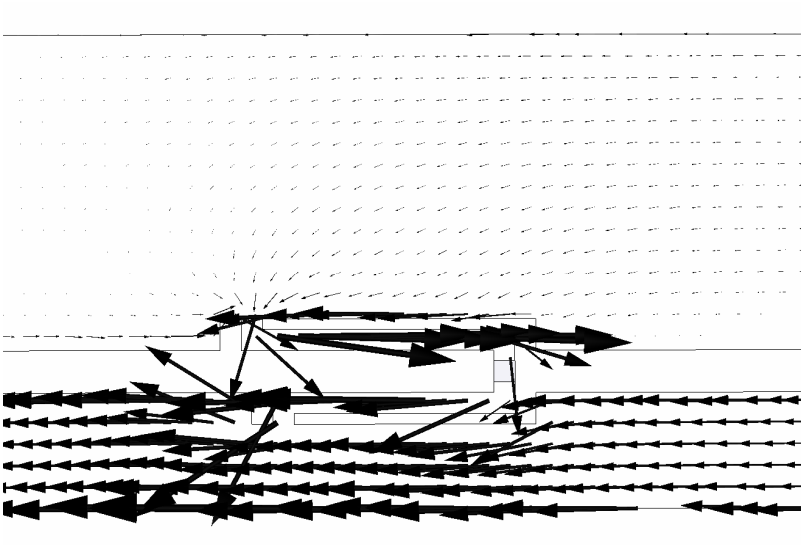

Fig. 13: Surface currents at 0g/100g

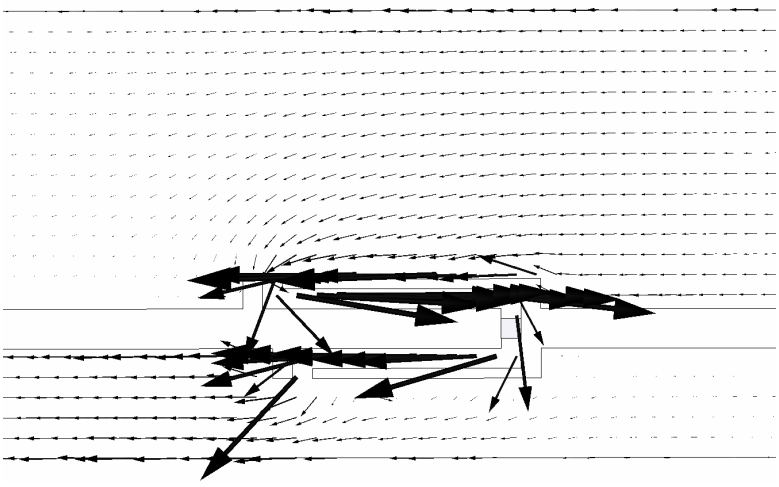

Fig. 14: Surface currents at 10g/100g

4. Measured Results

4.1. Measured Impedance

Impedance of the proposed antenna design was measured at various water contents given in Table 2 using a network analyzer. We used a 1:2 chip BALUN, mounted on a PCB, with the unbalanced end connected to the network analyzer and the balanced end probing the mounting pads of the antenna. The measured impedance is plotted in a power wave Smith chart shown in Figure 15. As in Figure 10 impedance is plotted between 890 MHz and 940 MHz at 2 MHz intervals. The solid square indicates the impedance at 890 MHz for all the water contents.

Comparing the simulated impedance in Figure 10 and the measured impedance in Figure 15, we can see that there is fairly good agreement between the two in terms of the resonant frequencies. We can clearly see that the imaginary part of the measured and simulated impedances has a very good agreement. The real part of the measured impedance is consistently slightly larger than the simulated impedance as the impedance gets very small. This can be attributed to error in calibration of the network analyzer at very low impedances. It also should be noted that the visual differences between the measured and simulated impedance is exaggerated at very low impedances due to the normalization of the Smith chart according to (3).

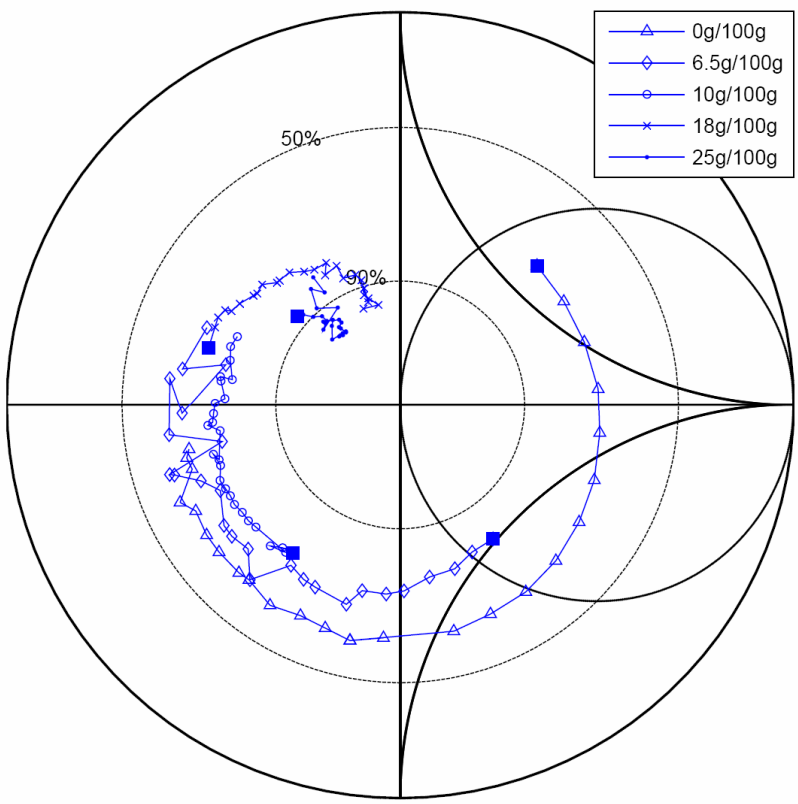

Fig. 15: Measured impedance plotted in a power wave Smith chart normalized to 35-j110 Ω

4.2. Measured Performance

The antenna performances were measured using an indirect method. Equation (9) is the Friss transmission equation that includes the power transfer efficiency τ and the polarization mismatch ρ in order to fit for an RFID system [18]. P_r is the received power, P_t is the transmitted power, G_r is gain of the receive antenna, G_t is gain of the transmit antenna, λ is the wavelength, R is the distance between the transmit antenna and the receive antenna. G_r in (9) is the gain over the accepted power of the antenna also given by (10).

$$\frac{P_r}{P_t} = G_t G_r \left(\frac{\lambda}{4\pi R} \right)^2 \tau\rho \tag{9}$$

$$G_r = D\eta \tag{10}$$

Now using (9), (10) and (5) the realized gain G_R of an antenna with a complex load can be obtained as (11).

$$G_R = \frac{P_r}{P_t G_t} \left(\frac{4\pi R}{\lambda} \right)^2 \frac{1}{\rho} \tag{11}$$

In order to measure the realized gain G_R for the antenna shown in Figure 6 we first fabricated the antenna and then attached an RFID chip to the antenna to form an RFID tag. The tag was then placed in front of a Samsys MP9320 reader antenna at a distance of 1 meter and the tag is read at different frequencies for various power levels. The lowest transmit power at which the tag can be read is recorded. This power is taken as P_t in (9). This is the power at which the chip receives nothing more that its turn on power (TOP) which is a published quantity. This TOP is taken as P_r in (9). Now we have all the information required to obtain G_R using (11).

Two sets of corrugated fiberboard samples at all the water contents shown in Table 2 were made. One set of corrugated fiberboard samples was used to make the proposed tag antenna. The realized gain of the tag antenna was obtained using the method discussed above. The tag was placed on corrugated fiberboard samples of all the water contents given in Table 2 with a metal foil backing. The second set of corrugated fiberboard samples was used to measure the performance of Avery Dennison's AD-612 tag (140

mm×24 mm) using the same method. The AD-612 tag was selected for comparison because it is a tag that is intentionally tuned to work well in proximity to metal [19]. The same AD-612 tag was used for all the water contents in order to avoid variance due to different chips.

The performance graph obtained is given in Figure 16. Realized gain measurements at 915 MHz, realized gain simulated at 915 MHz and the AD-612 tags realized gain measurements at 915 MHz are plotted in the same graph for comparison. We observe that performance of the AD-612 tag in abnormal humidity conditions is highly degraded when compared to the dual resonant tag proposed. The dual resonant tag has a fairly consistent performance over different water contents and also performs much better than AD-612 in all water contents.

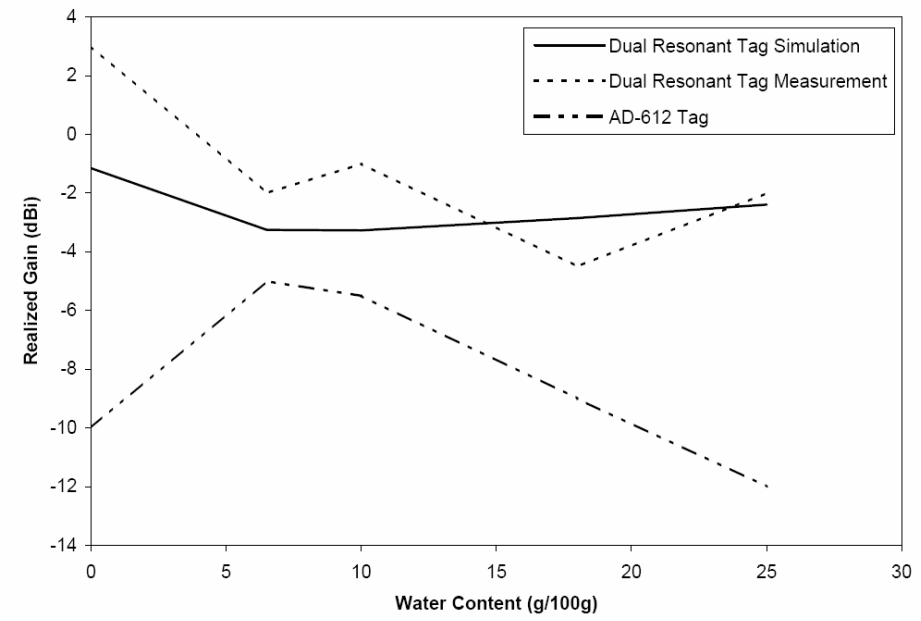

Fig. 16: Measured gain realized

The measured performance follows the simulated performance fairly well. There are variations between simulated and measured performance. These variations can be attributed to a number of factors; first, measurements using Samsys reader has a 0.5 dB resolution and hence the accuracy of all the measurements is at least ±0.5 dB. Second, different RFID chips were used with each antenna sample. The chips have an inherent variance of turn on power that might affect the overall performance of the tag. Third, there may be inaccuracies in fabrication of the antenna. Fourth, there may be inconsistency in acrylic adhesives used to attach the antenna and ground plane to the corrugated fiberboard samples.

E-Plane and H-Plane radiation patterns of the tag were measured in room temperature conditions at 915 MHz and are given in Figure 17. The measured radiation pattern is a validation that the surface currents behave as expected from simulation.

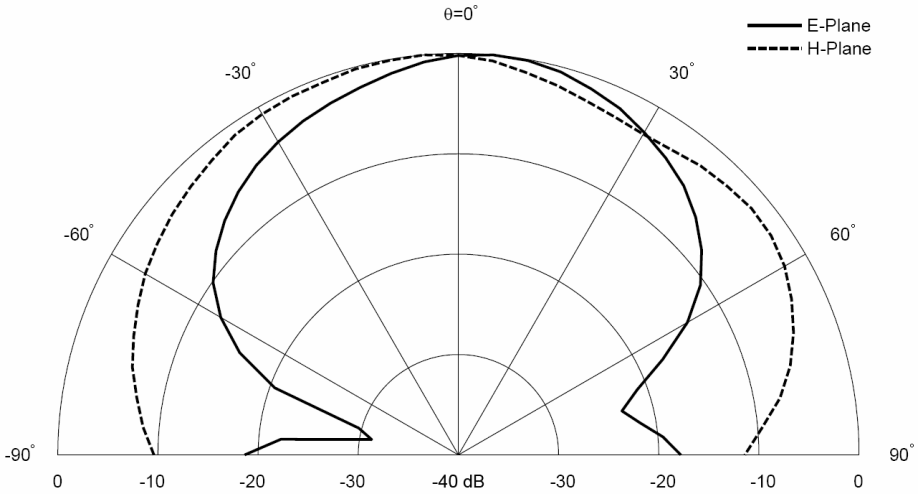

Fig. 17: E and H Plane directivity pattern (peak normalized to 0 dB)

5. Conclusion and Future Work

In this thesis we presented a novel planar dual-resonant microstrip antenna using corrugated fiberboard as a substrate. The proposed antenna was designed to effectively eliminate the content sensitivity, moisture sensitivity and the near-far problem. By eliminating these limitations the tag proves to be a uniquely good solution that enables the use of UHF RFID to efficiently track goods in the cold chain.

We presented simulated and measured impedance for the proposed tag antenna design at various water contents i.e. temperature and humidity conditions using the power wave Smith chart. We also presented the tag's performance measurements with a Monza 1 Gen 2 RFID chip using the Samsys MP9320 reader at various water contents and we also compared the performance with a commodity tag that uses the same chip and has a comparable form factor.

We showed simulated and measured results that clearly indicate there is a significant improvement in maintaining a constant performance over various water contents when using the proposed dual resonant microstrip antenna due to the clear advantage of higher. The performance obtained met the design requirements we specified.

The proposed antenna design also has a form factor that has the potential to be manufactured inexpensively and in very high numbers using

readily available techniques thus meeting the physical dimension constraints for a tag intended to be used in the cold chain application.

Thus, we conclude that the proposed dual resonant antenna and feed structure is a highly promising UHF RFID tag antenna solution that is cost-effective, leverages the readily available UHF RFID infrastructure and enables rapid product recall in the cold chain.

Although we have proved the feasibility of the proposed dual-resonant antenna, there is still room for improvement. The width of Patch 2 can be increased further by compromising width of Patch 1, so that, $G_R(25g/100g)$ is increased further resulting in an overall increased performance level. Also, the same antenna design technique may be used to obtain an antenna with a smaller form factor by compromising performance of the tag antenna equally over the various water contents. The analysis presented here was done in room temperature conditions. A more thorough analysis of the dielectric properties of corrugated fiberboard at different temperature conditions is required to understand the complete dielectric range of corrugated fiberboard.

6. References

[1] Federal Oversight of Food Safety: High-Risk Designation Can Bring Attention to Limitations in the Government's Food Recall Programs http://www.gao.gov/new.items/d07785t.pdf April 24, 2007.

[2] Keeping Fresh Foods Fresh: RFID Journal, http://www.rfidjournal.com/magazine/article/2137 .

[3] M. E. Parker, J. E. Bronlund, A. J. Mawson., "Moisture sorption isotherms for paper and paperboard in food chain conditions," Packaging Technology and Science, Vol.19, No.4, pp.193-209, Feb.2006.

[4] Marcondes J., "Corrugated fibreboard in modified atmospheres: moisture sorption/desorption and shock conditioning," Packaging Technology and Science, vol.9, no.2, pp.87-98, Dec. 1996.

[5] Marcondes, et al. "Cushioning properties of corrugated fibreboard and the effects of moisture content," Transactions of the ASAE, Vol. 35, No.6, pp.1949-1953, 1992.

[6] H. Kwon, B. Lee: "Compact slotted inverted-F RFID tag mountable on metallic objects," IEE Electronic Letters, vol. 1 pp 1308-1310, November 2005.

[7] Ukkonen, L., Engles, D., Sydanheimo,L., and Kivikoski, M., "Planar Wire- type Inverted-F RFID tag Antenna mountable on metallic objects."

Antennas and propagation society International symposium Vol. 1, pp 101 – 104, 2004.

[8] M. Eunni, M. Sivakumar, D. D. Deavours. “A Novel Planar Microstrip Antenna Design for UHF RFID.” JSCI, vol. 5, no. 1, pp. 6-10, January 2007.

[9] Supreetha Rao Aroor and Daniel D. Deavours. Evaluation of the State of Passive UHF RFID: An Experimental Approach. *IEEE Systems Journal*, to appear.

[10] Madhuri Eunni, A Novel Planar Microstrip Antenna Design for UHF RFID, Master’s Thesis: Department of Electrical Engineering and Computer Science, University of Kansas, July 2006.

[11] Pavel V. Nikitin, K. V. Seshagiri Rao, Sander F. Lam, Vijay Pillai, Rene Martinez, and Harley Heinrich, “Power Reflection Coefficient Analysis for Complex Impedances in RFID Tag Design,” IEEE Transactions on Microwave Theory and Techniques, Vol. 53, No. 9, Sep 2005.

[12] K. Kurokawa, “Power waves and the scattering matrix,” IEEE Transactions on Microwave Theory and Techiques, vol. MTT-13, no. 3, pp. 194–202, Mar. 1965.

[13] Constantine A. Balanis, Antenna Theory Analysis and Design, New Jersey: Willey, 2005.

[14] Johan C.-E. Sten, Arto Hujanen, and Päivi K. Koivisto, “Quality Factor of an Electrically Small Antenna Radiating Close to a Conducting Plane,” IEEE Transactions on Antennas and Propagation, Vol. 49, No. 5, pp.829-837, May 2001.

[15] Randy Bancroft, Microstrip and Printed Antenna Design, Atlanta: Noble Publishing, 2004.

[16] David M. Pozar, Microwave Engineering, New York: John Wiley & Sons, 1988.

[17] Ansoft Corporation, HFSS Online Help, Pittsburg, PA, 2006.

[18] K. V. Seshagiri Rao, Pavel V. Nikitin, Sander F. Lam, "Antenna Design for UHF RFID Tags" A Review and a Practical Application," IEEE Transactions on Antennas and Propagation, Vol.53, No. 12, pp. 3870-3876, Dec 2005.

[19] Avery Dennison RFID, AD-612 RFID Inlays, http://www.webermarking.com/images/Avery_612.pdf